

Microwave-induced adjustable nonlinear temperature gradients in microfluidic devices

This article has been downloaded from IOPscience. Please scroll down to see the full text article.

2010 J. Micromech. Microeng. 20 105025

(<http://iopscience.iop.org/0960-1317/20/10/105025>)

View [the table of contents for this issue](#), or go to the [journal homepage](#) for more

Download details:

IP Address: 129.6.65.219

The article was downloaded on 30/09/2010 at 15:07

Please note that [terms and conditions apply](#).

Microwave-induced adjustable nonlinear temperature gradients in microfluidic devices

Jayna J Shah¹, Jon Geist and Michael Gaitan

National Institute of Standards and Technology, Semiconductor Electronics Division,
100 Bureau Dr. Stop 8120, Gaithersburg, MD 20899, USA

E-mail: gaitan@nist.gov and jjshah@ieee.org

Received 22 March 2010, in final form 9 August 2010

Published 29 September 2010

Online at stacks.iop.org/JMM/20/105025

Abstract

We describe on-chip microwave generation of spatial temperature gradients in a polymeric microfluidic device that includes an integrated microstrip transmission line. The transmission line was fabricated photolithographically on commercially available adhesive copper tape. The fluid temperature during microwave heating was measured by observing the temperature-dependent fluorescence intensity of a dye solution in the microchannel. Large interference effects, which were produced by superposition of a sinusoidal and two exponential temperature distributions, were measured at 12 GHz and 19 GHz. Temperature extremes of 31 °C and 53 °C at the minimum and maximum of the sinusoid were established within 1 s. The sinusoid also produced a quasilinear temperature gradient along a 2 mm distance with a slope of 7.3 °C mm⁻¹. This technique has the potential to benefit many biological, chemical and physical applications requiring rapid temperature gradients.

(Some figures in this article are in colour only in the electronic version)

1. Introduction

Integrated microfluidic devices require a number of functionalities such as mixing, pumping and valving for high-throughput chemical and biological applications [1–3]. Much work has been done in the recent years to perform some of these tasks on-chip [2, 4, 5]. Temperature control inside microfluidic devices is another crucial function as generally all biochemical processes are temperature driven and it still remains a challenge. Indeed, spatial and temporal temperature gradients have attracted a lot of attention for a variety of on-chip applications, including investigation of thermophoresis [6], control and measurement of enzymatic activity [7–9], investigation of the thermodynamics [10, 11] and of the kinetics characterizing molecular associations [12, 13]. Additionally, miniaturization of chemical analysis systems for higher throughput and efficiency necessitates the detection of very dilute solutions of analytes in ultra small volumes, nanoliters or less. A number of preconcentration as well as chemical separation methods have been investigated that

rely on a well-controlled and well-defined temperature field [14–17].

Thus far, most efforts toward generating temperature gradients have focused on a one-dimensional heat flow between a heat source and a cold sink leading to a linear gradient in temperature between the two [18]. The vast majority of approaches use bulk heaters [11] attached to microfluidic substrates such as aluminum heating plates [14, 17, 19], copper heating/cooling blocks [16, 20] and peltier elements [21]. The limitations associated with these approaches include heating of large substrate areas possibly preventing the integration of multiple analysis functions on a single substrate. Alternative techniques have been developed to improve temperature localization and minimize footprints. Most techniques for generating on-chip temperature gradients integrate Joule heating elements to conduct heat into microchannels/microchambers [7, 14, 22]. However, temporal control is limited by the heat capacity of the microfluidic device and thermal coupling of the device to the heating elements.

¹ Author to whom any correspondence should be addressed.

Microwave electric fields, on the other hand, have attracted much attention for a number of on-chip heating as well as sensing applications. For example, transmission lines have been integrated with microchannels to heat water as well as saline solutions using continuous wave microwave power [23, 24]. Equations have been derived to describe the absorption of microwave power in different regions of low-reflectance transmission lines used for heating microchannels [25]. Microwave-mediated thermocycling has been demonstrated in microfluidic wells designed to terminate microwave energy for DNA amplification applications [26–28]. Further, microwave transmission lines have been used for on-chip dielectric permittivity and spectroscopy measurements [29–32]. AC electric fields have also been used at microwave frequencies for electrothermal actuation of water [33, 34]. More recently, localized microwave heating of fluids has been described in the vicinity of sensor–heater silicon field effect transistors [35, 36], and microwave dielectric heating of insulated water drops has been demonstrated in microfluidic systems [37].

In this paper, we present a technique to locally and rapidly generate temperature gradients within microchannels using microwave electric fields. The temperature distribution in the channel fluid is proportional to the time average of the square of the microwave electric field, which contains a sinusoidal component in the presence of a standing wave in the transmission line. This phenomenon is similar to the sinusoidal darkening of a thin layer of photo-sensitive collodion described in Wiener’s classic demonstration that photochemistry is sensitive to the electric field rather than the magnetic field of electromagnetic radiation [38]. In our devices, a nonlinear sinusoidally shaped gradient along a 7 mm distance with fluid temperatures as large as 53 °C and as low as 31 °C and a quasilinear temperature gradient with a slope of 7.3 °C mm⁻¹ can be achieved within 1 s. The electric field distribution can also be controlled via the operating frequency and input power, which provides flexibility in changing the temperature profile for different specimens, reactions or applications.

2. Model of temperature gradient generation

The power density in a dielectric material upon exposure to alternating electromagnetic field is given by [39]:

$$P = \omega \epsilon_0 \epsilon''(\omega) |E|^2, \quad (1)$$

where ω is the angular excitation frequency, ϵ_0 is the vacuum permittivity, ϵ'' is the loss factor and E is the electric field strength in volts per meter within the material. For a wave traveling in the z -direction on a transmission line, the phasor representation of the total electric field is the sum of contributions from two separate components, the forward wave and the reflected wave, as described below:

$$E(z, t) = |E_+| e^{-jkz} e^{j\omega t} + |E_-| e^{jkz} e^{j\theta_p} e^{j\omega t}, \quad (2)$$

where $jk = \alpha + j\beta$, E_+ is the amplitude of the forward wave, k is the complex propagation constant, E_- is the amplitude of the reflected wave, θ_p is the phase angle between the reflected

and forward waves, α is the attenuation constant that describes the rate of decay of microwave power per unit length, z is the distance along the direction of propagation and β is the phase constant (change in phase per unit length) [40]. The time-averaged power density $\langle P \rangle$ is proportional to $E(z, t) \cdot E(z, t)^*$. Thus, we can compute the temperature profile of the fluid in the microchannel according to

$$T = a^2 e^{-2\alpha z} + b^2 e^{2\alpha z} + 2ab \cos(2|\beta|z + \theta_p), \quad (3)$$

where T is the fluid temperature due to microwave heating.

This simplified model describes several key features of microwave-induced temperature gradients. The dielectric properties of the transmission medium are non-homogeneous due to the presence of the microchannel resulting in impedance mismatch at the boundaries of the microchannel. The constructive and destructive interference caused by impedance mismatch between the forward and reflected waves at these boundaries generate a standing wave in the electric field and a corresponding stationary temperature field within the microchannel. The shape and magnitude of the temperature field depends on the microchannel geometry, the position of the microchannel relative to the transmission line, the frequency of operation and the input power. The rate of decay of the temperature field is governed by the transmission-line attenuation factor α , which is a function of the transmission-line geometry and the frequency-dependent loss factors of the transmission line materials. Hence, the higher the operating frequency of the microwave electric field, the lower the wavelength of the temperature field producing more peaks and valleys in the spatial temperature profile, and the higher the attenuation constant, the higher the average slope in the temperature field from the front to the back of the channel.

3. Experimental details²

3.1. Chemicals and materials

Cyclic olefin copolymer (COC) was obtained from Plitek, LLC (Des Plaines, IL). Copper tape with non-conducting acrylic adhesive (Permacel P-389) was obtained from Electrical Insulation Suppliers, Inc. (Philadelphia, PA). Rhodamine B was purchased from Alfa Aesar (Ward Hill, MA).

3.2. Device fabrication

Figure 1 shows a cross-sectional schematic and a picture of the microwave-heated microfluidic device used in this work. The devices were fabricated using an adhesive copper tape on COC using photolithographic procedures. A CNC milling machine (Protomat S62, LPKF Laser & Electronics AG, Garbsen, Germany) was used to cut the substrate material to precise chip dimensions and to carve out the microchannel and the fluidic access ports. The microchannel was 340 μ m wide, 7 mm long and was machined all the way through in a

² Certain commercial equipment, instruments or materials are identified in this paper to specify the experimental procedure adequately. Such identification does not imply recommendation or endorsement by the National Institute of Standards and Technology, nor does it imply that the materials or equipment identified are necessarily the best available for the purpose.

300 μm thick COC substrate. The channel was positioned 1 cm away from the front of the device. The signal line was 370 μm wide and 5 cm long. The signal line and the ground plane were patterned on the copper tape after the tape was fixed on the top and bottom surfaces of the COC substrate. The tape had a 40 μm thick acrylic adhesive on a 35 μm thick copper foil. The acrylic adhesive served as a cover plate for the microchannel and isolated the fluid from the copper electrodes. A slit, 100 μm wide and 2 cm long, was fabricated in the ground plane to allow optical detection of the fluid for temperature measurement.

The dimensions of the microchannel, the transmission line and the slit were determined from electromagnetic simulations performed using Sonnet (Sonnet Software, North Syracuse, NY). The slit was designed to run parallel to the microchannel, and it was positioned in the middle of the microchannel (figure 1(b)) with a photolithographic process. Such positioning allowed for spatially resolved, optical fluid-temperature measurements throughout the length of the microchannel and laterally in the middle of the channel. Two 2.4 mm end-launch connectors were mounted on the device (figure 1(a)) to convert from the microstrip geometry to the coaxial geometry of the test equipment.

3.3. Device characterization

Two types of measurements were made to characterize the device: scattering (S) parameters and temperature. S -parameters describe the forward and reflected power and/or voltage waves in a transmission medium and can be used to model the power flow as a function of frequency through the device. We used the S -parameter data to determine the power absorbed in the fluid and to select appropriate frequencies for generating temperature gradients.

3.3.1. Frequency response measurements. The broadband frequency response of the devices was determined from the transmission and reflection-coefficient S -parameter measurements, which were obtained using a vector network analyzer (N5230A, Agilent Technologies, Santa Clara, CA). A full two-port Short-Open-Load-Thru (SOLT) calibration was performed using commercially available 2.4 mm calibration standards (85056D, Agilent Technologies) [41]. The reference plane for the calibration was set at the end of the microstrip to coax connectors.

3.3.2. Temperature measurements. The electronics that generate the microwave energy for the temperature gradient measurements were assembled as shown in figure 1(c). The microwaves were generated at a frequency of interest using the signal generator (E8257D, Agilent Technologies) and amplified to a maximum of 30 dBm (1 W) with a solid-state power amplifier (L0220, Microwave Power, Inc., Santa Clara, CA). The amplifier was powered using a dc power supply (E3615A, Hewlett Packard) and pulsed with an arbitrary waveform generator (33250A, Agilent Technologies). The microwave power transmitted out of the device was terminated by connecting a power sensor (8485A, Agilent Technologies)

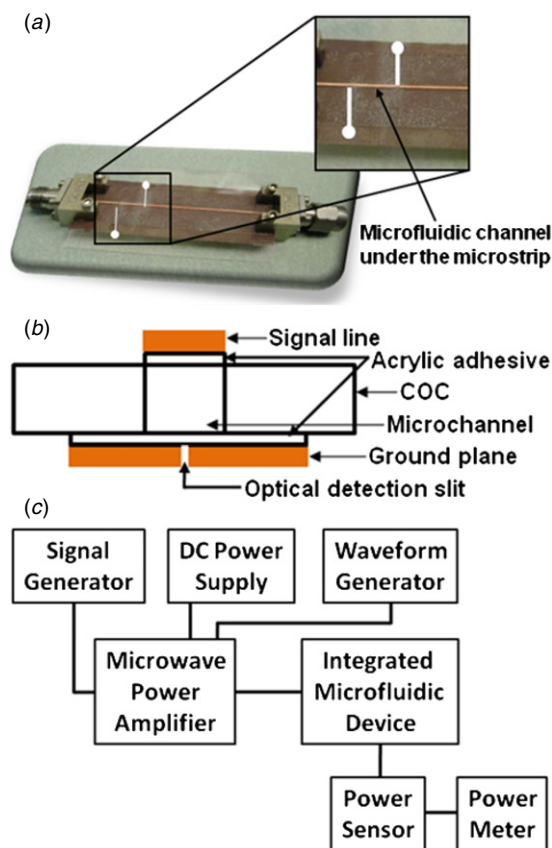


Figure 1. (a) A picture of the integrated microfluidic device for generating microwave-induced temperature gradients. The inset shows a microchannel highlighted in white that is sandwiched between the signal and ground metal conductors of a microwave transmission line. The 2.4 mm end launch connectors are used to convert from microstrip to coaxial geometry. (b) A cross-sectional view of the microwave heating device. The microstrip transmission line is integrated with a cyclic olefin copolymer (COC) substrate containing a microchannel. The substrate is 3 cm wide and 5 cm long. The metal conductors are 35 μm thick, the signal line is 370 μm wide and the ground plane is 1.8 cm wide. The channel cover plates are made of 40 μm thick acrylic adhesive. A slit, 100 μm wide and 2 cm long, is fabricated into the ground plane for optical detection of the microchannel fluid. (c) A schematic of the experimental setup used for microwave-induced temperature gradient measurements.

at the output port of the integrated microfluidic device, while a power meter (E4419B, Agilent Technologies) connected to the power sensor was used to measure the transmitted power. The fluid was heated by pulsing the microwave power over a 12 s period with an 8.33% duty cycle.

The fluid temperature was measured remotely by observing the temperature-dependent fluorescence intensity of a dilute fluorophore added to the fluid and comparing it to the calibrated fluorescence intensity at a known temperature. Rhodamine B is one of a class of fluorescent dyes with a temperature-dependent quantum yield that can be used to obtain temperature profiles by observing the relative spatial and temporal intensity changes using a previously described fluorescence imaging technique [42]. We used an aqueous solution of 0.2 mmol L⁻¹ Rhodamine B dissolved in a

19 mmol L⁻¹ carbonate buffer to demonstrate the presence of temperature gradients.

The temperature profile was constructed by measuring the fluorescence intensity throughout the microchannel in 0.5 mm increments starting at the beginning of the channel, close to the input port of the device, while the microwave power was pulsed as described earlier. The position was determined manually by a screw-drive actuator mounted on the stage of a microscope. The uncertainty of the position measurement was $\pm 25 \mu\text{m}$.

A Zeiss Axiovert 25 inverted fluorescence microscope (Carl Zeiss MicroImaging, Inc., Oberkochen, Germany) with a 20 \times objective with a Rhodamine B filter set (excitation: band pass 525 nm/40 nm, emission: band pass 585 nm/40 nm) and a broadband mercury arc lamp were used for illumination. Twelve-bit, 90 \times 30 pixel grayscale intensity images were captured at a rate of 140 frames s⁻¹ using a CMOS camera-link camera (MV-D1024E, Photonfocus AG, Lachen, Switzerland) at a typical exposure time of 7 ms. The camera gain was set manually and kept constant throughout a given set of temperature measurements. Digital images were acquired using an image acquisition board (PCIe-1427, National Instruments Corp., Austin, TX) with a PCI Express bus capable of data transfer rates of greater than 200 MB s⁻¹.

Microwave power delivery, image acquisition, and storage were controlled by LabVIEW software (National Instruments Corp.). The images were analyzed using MATLAB (The MathWorks, Inc.). A total of 4000 frames were captured over approximately a 50 s time period at each position, which included three microwave pulse cycles. For temperature extraction, the frames were first analyzed pixel by pixel for the removal of any hot pixels inherent in the camera when the illumination light was off and any pixels that became saturated during heating. The average intensity value was then calculated for each frame. Finally, the intensity values obtained during heating were normalized to the intensity when the power was off.

The temperature from the normalized fluorescence intensity ratio was obtained using the cubic equation

$$T = A_0 + A_1 I + A_2 I^2 + A_3 I^3, \quad (4)$$

where T is the temperature and I is the fluorescence intensity normalized by its room temperature value ($21.7 \text{ }^\circ\text{C} \pm 0.7 \text{ }^\circ\text{C}$). The coefficients ($A_0 = 141.53$, $A_1 = -250.25$, $A_2 = 228.02$ and $A_3 = -96.904$) were obtained from a previously published calibration [43]. For our system, we had experimentally determined that the fluorescence was being collected from an absorbed layer of dye molecules in the acrylic adhesive rather than from the bulk of the fluid, making our experimental conditions similar to that of Samy *et al* [43] where the normalized fluorescence intensity was computed from dye molecules absorbed in a poly(dimethylsiloxane) (PDMS) thin film.

4. Results and discussion

The choice of materials, COC and Cu tape, along with our fabrication method offers several advantages for producing

integrated microfluidic devices for microwave heating. The high glass transition temperature of COC ($T_g = 136 \text{ }^\circ\text{C}$) as well as its chemical compatibility with acids, alcohols, bases and polar solvents make it suitable for photolithographic procedures. While the low thermal conductivity of COC ($0.135 \text{ W m}^{-1} \text{ K}^{-1}$) has a negative impact for contact heating approaches, it offers a significant advantage for direct volumetric-based heating strategies by minimizing undesired heat losses, so that a larger fraction of the incident power is contained in the fluid during heating. Additionally, the low dielectric constant ($\epsilon_r = 2.35$) and the low loss factor ($\tan \delta = \sim 1 \cdot 10^{-4}$ at 10 GHz) of COC make it suitable for high-frequency applications such as the one demonstrated in this report.

The use of electro-deposited Cu compared to metal alloys as in the low-melt solder fill technique [44], e.g. a combination of indium-bismuth-tin alloy [37], for forming the transmission-line electrodes permitted high-frequency operation of our devices due to the high electrical conductivity ($\sigma_{Cu} = \sim 5.51 \times 10^5 \text{ S cm}^{-1}$, $\sigma_{Indalloy} = 0.19 \times 10^5 \text{ S cm}^{-1}$) of Cu. On the other hand, the conductor thickness in our devices exceeded the thickness ($3\delta = 2 \mu\text{m}$ at 10 GHz for Cu, where δ is the skin depth) needed to sufficiently suppress ohmic losses due to the skin effect, and the greater-than-required thickness of Cu ($35 \mu\text{m}$) acted as a thermal heat sink, limiting the maximum achievable temperature in the microchannel.

The method described here for fabricating conductors is easily transferable to other microfluidic substrates such as glass and PDMS. Furthermore, our one-step method for conductor fabrication obviates the need for electroplating, which is typically required following thin-film deposition to achieve sufficient conductor thickness. Our method also provides easy bonding of the top and bottom cover plates to create enclosed channel structures, which has proven challenging for thermoplastic materials [45]. In contrast to previously published reports [23, 29, 30], the transmission line structure shown in this work isolates the fluid from the metal conductors making these devices suitable for a variety of biochemical applications in which reagent contamination due to electrolysis or corrosion is undesirable.

An electromagnetic simulation of a geometrical structure similar to that shown in figure 1(a) was performed using Sonnet with nominal properties for copper, acrylic, COC and water. The design parameters were varied to optimize microwave power absorption in the fluid since absorption governs the maximum attainable temperature. A trade-off relation was found to exist between the power absorbed in the fluid and the ratio of the channel height to the total substrate thickness (the sum of cover plates and COC thickness). A smaller channel height to substrate thickness ratio reduced the absorbed power for a given fluid volume and incident microwave power.

The coupling of the microwave power from the amplifier (less than, but approximately equal to 1 W) to the transmission line and the microchannel was characterized theoretically and experimentally by measuring the reflection coefficient (S_{11}) and the transmission coefficient (S_{21}) and by calculating the absorption ratio ($A = 1 - |S_{11}| - |S_{21}|$), which describes the fraction of the incident power absorbed by the device, where

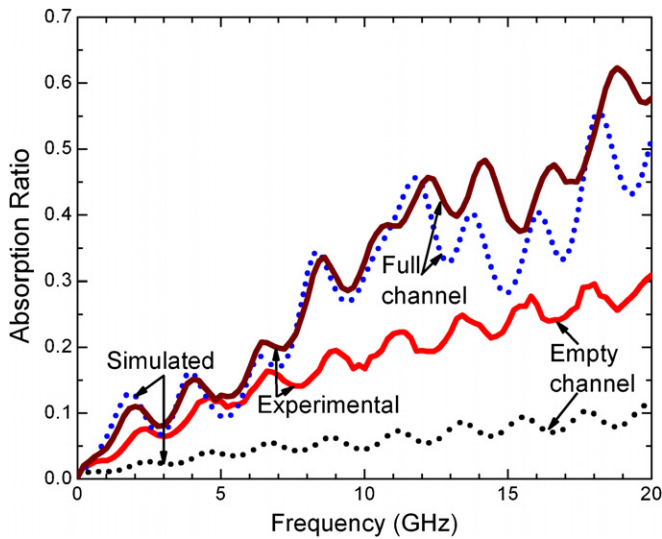


Figure 2. Comparison between simulated and measured absorption ratios, the fraction of the incident microwave power absorbed by the device, as a function of frequency. The simulated and measured responses are compared for the empty channel as well as the water-filled device. The curves are constructed from S -parameter data according to $A = 1 - |S_{11}| - |S_{21}|$, where S_{11} is the reflection coefficient and S_{21} is the transmission coefficient. (●●●, upper dotted line) Simulated full channel response, (—, upper solid line) measured full channel response, (—, lower solid line) measured empty channel response, (●●●, lower dotted line) simulated empty channel response.

$S_{ij}(\text{dB}) = 10\log_{10}|S_{ij}|$. Figure 2 shows the simulated and measured absorption ratios for the empty-channel and water-filled device. Close agreement is found in both the amplitude and shape for the full-channel device, but only in shape for the empty-channel device with the correlation coefficient of 0.98 for the empty-channel device and 0.96 for the water-filled device. The amplitude deviation in the experimental absorption ratio for the empty-channel device can be attributed to imperfections in the as-fabricated conductor. However, this difference is much smaller for the water-filled device apparently because fluid absorption dominates the absorptive process.

The S -parameter information was also used to select frequencies where large sinusoidally shaped temperature gradients were expected. Specifically, we found that constructive interference exists between the traveling and reflected waves at a frequency corresponding to local maxima in the absorption ratio curve for the water-filled device. The absorbed power increases with increasing frequency, and the peaks in the absorbed power exist at a variety of frequencies (figure 2). However, the amplitude of the absorbed power at the peaks for frequencies lower than 12 GHz is significantly smaller than that at 12 GHz and above. Here, we show the results of temperature measurements at the lowest (12 GHz) and highest (19 GHz) frequencies that gave relatively large peaks in the absorption ratio data.

Figure 3 shows the experimental temperature profile for the excitation frequency of 19 GHz. The curve in figure 3 was constructed by using the calibration curve of Rhodamine B dye to convert the fluorescence intensity into temperature. We

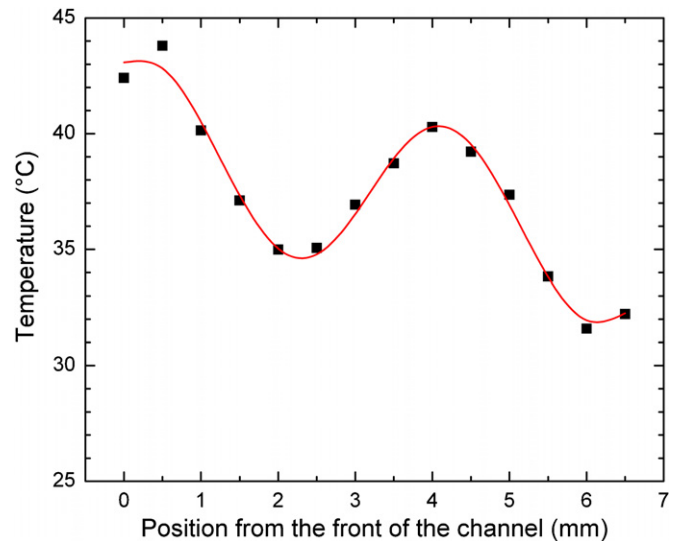


Figure 3. The measured temperature versus distance along the microchannel of an aqueous solution of 0.2 mmol L^{-1} Rhodamine B in a 19 mmol L^{-1} carbonate buffer at the microwave excitation frequency of 19 GHz. The solid line represents a theoretical temperature fit to the measured data points shown in squares. The measurement frequency was selected based on a local maximum in A for the full channel device. At 19 GHz, $S_{11} = 0.040$, $S_{21} = 0.343$ and $A = 0.617$ for the full channel device.

Table 1. Results from nonlinear least-squares fitting of the temperature gradient model (equation (3)) to the measured data points shown in figures 3 and 4 for one device. A standard error of zero indicates that this value was fixed during the fit.

	12 GHz		19 GHz	
	Value	SD	Value	SD
a (V mm^{-1})	6.986	0.051	6.310	0.024
b (V mm^{-1})	0.501	0.041	-0.281	0.017
β (deg mm^{-1})	29.11	0	46.35	0.974
θ_p (deg)	264.8	3.25	154.1	7.071
α (mm^{-1})	0.015	0.002	0.010	0.001
Chi-square	1.193	-	0.257	-
R^2	0.975	-	0.981	-

observed a nonlinearly modulated profile extending along the length of the microchannel. We compared the temperatures measured at different positions with our model of temperature gradient generation by performing nonlinear least-squares fitting of equation (3) to the measured data points using Origin software (solid line in figure 3) and found good agreement ($R^2 = 0.98$). The parameter estimates and the associated standard errors are listed in table 1.

For a given geometrical structure, the nonlinear temperature profile (figure 3) can be altered by changing the frequency of the microwave signal. This is demonstrated in figure 4, which shows the spatial temperature profile obtained for 12 GHz excitation frequency. Here, we observed a nonlinear profile representing a sinusoidal wave extending along the length of the microchannel. Our data also resulted in a quasilinear temperature gradient with a slope of $7.3 \text{ }^\circ\text{C mm}^{-1}$ along a 2 mm distance. Linear temperature gradients with comparable slopes have been used for DNA

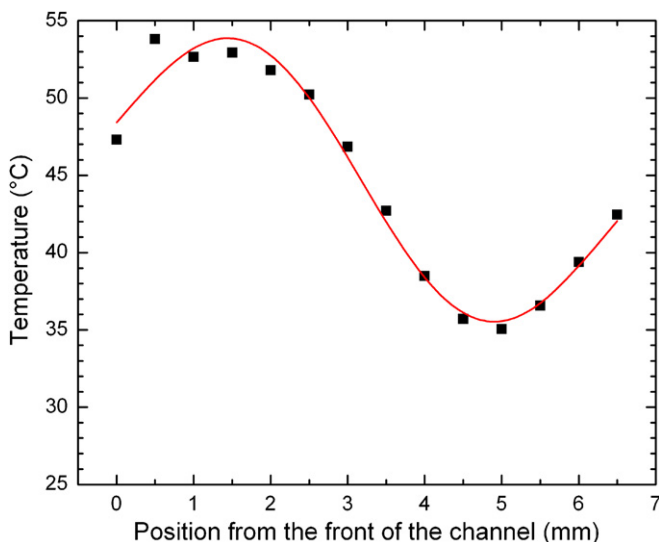


Figure 4. The measured temperature of an aqueous solution of 0.2 mmol L^{-1} Rhodamine B in a 19 mmol L^{-1} carbonate buffer as a function of position along the microchannel at the microwave excitation frequency of 12 GHz. The solid line represents a theoretical temperature fit to the data points in squares. The measurement frequency was selected based on a local minimum in S_{11} (not shown here) and a local maximum in A for the full channel device. At 12 GHz, $S_{11} = 0.063$, $S_{21} = 0.490$ and $A = 0.447$ for the full channel device.

mutation detection [17], phase transition measurements in phospholipid membranes [8], single-nucleotide polymorphism (SNP) analysis [11] and continuous-flow thermal gradient PCR [19]. As before, nonlinear least-squares fitting of the theoretical model (solid line in figure 4) to the experimental data shows good agreement ($R^2 = 0.98$). Due to limitations of our temperature gradient model, the fit to the 12 GHz data was not able to estimate the attenuation constant, α , with reasonable uncertainty because of multicollinearity (all of the coefficients of the covariance matrix were >0.8). Therefore, we performed the fit to 12 GHz data by fixing β (table 1). The value of β that we used was obtained from the fit to 19 GHz data by assuming that dispersion was negligible and scaling appropriately for the ratio of the two frequencies.

One noteworthy application of a rapid, nonlinear temperature (electric field) gradient is electric field gradient focusing (EFGF) of charged molecules. It has been suggested theoretically that the peak capacity and resolution of EFGF and other related methods, such as TGF [16], could be increased by using a nonlinear field (temperature) gradient provided that the first portion of the gradient is steep, the following section is shallow and that the sample components can be moved from the first portion to the second after focusing in the first portion [46, 47]. It should be possible to optimize our experimental setup to produce temperature gradients that meet these requirements.

To demonstrate the efficacy of our technique for generating temperature gradients, we performed measurements on several different devices (table 2). The general shape of the temperature gradient curve was found to reproduce well for all of the measurements. We also determined that the statistical deviations shown in the table

Table 2. The average and standard deviations of the fitting parameters extracted from nonlinear least-squares fitting of measured temperature gradient data to the theoretical model shown in equation (3) ($n = 6$ for 12 GHz data and $n = 5$ for 19 GHz data). A standard deviation of zero indicates that this value was fixed during the fit as described in the text.

	12 GHz		19 GHz	
	Mean	Average SD	Mean	Average SD
a (V mm^{-1})	6.912	0.049	6.427	0.035
b (V mm^{-1})	0.502	0.040	0.092	0.025
β (deg mm^{-1})	29.106	0.0	46.123	1.833
θ_p (deg)	259.4	3.229	193.6	14.22
α (mm^{-1})	0.011	0.002	0.012	0.002
Chi-square	1.142	–	0.712	–
R^2	0.971	–	0.923	–

come primarily from variations in the geometrical dimensions of the device introduced during the fabrication process.

Even though Rhodamine B dye was used successfully to demonstrate the presence of temperature gradients, accurate generation of the temperature gradient profile warrants improvements to the temperature detection method. In fact, a number of researchers have reported the specific absorption of Rhodamine B in PDMS substrates [43, 48]. In our experiment, Rhodamine B was found to absorb into acrylic adhesive resulting in temperatures that were representative of channel surface rather than that of the bulk fluid. Additionally, after repeated use the absorption resulted in non-uniform fluorescence intensity across the length of the microchannel indicating that the absorption was non-uniform in space which limited the reusability of our devices. Hence, our results demonstrate that while the method for generating spatial temperature gradients is robust as shown from the repeated measurements and low statistical error (table 2), the frequent use of our devices results in the channel surface becoming saturated with Rhodamine B dye limiting their overall use.

It should be possible to prevent the absorption of Rhodamine B dye on the microchannel surface by modifying those surfaces with appropriate surface treatments as is typically done for analyte separations in microfluidic devices [49]. Further, we also predict that a two-step process could be utilized to eliminate potential interactions of Rhodamine B dye with chemicals of interest. As the first step, a set of devices would be used with a dye solution to calibrate the temperature difference versus the microwave power characteristic of the device, and an identical device would be later used without the dye solution for performing biological or chemical studies. Alternatively, an electronic temperature sensor such as a thermocouple or resistance thermometer could be integrated into the device at a convenient reference location along the channel for optical calibration.

Figure 5 plots the temperature as a function of time at one location along the microfluidic channel for a 1 s duration pulse of approximately 1 W of microwave power applied to the device. Substantially, more power (about 1 W from the amplifier) was required to raise the temperature of the fluid to 46°C in 1 s than would be required to hold it at this temperature for an additional second as might be required

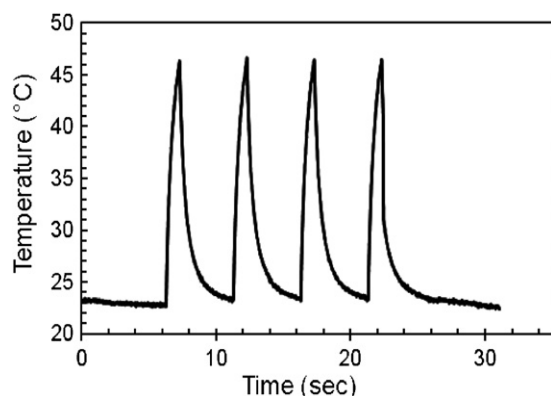


Figure 5. Transient temperature response of the integrated microfluidic device. A temperature of 46 °C was obtained at some locations in the microchannel with 1 W of microwave power at the output of power amplifier for 1 s. The fact that the temperature did not reach a steady state value in this time shows that considerably less power would be required to hold the temperature constant for a second. The addition of feedback control and a higher power amplifier would facilitate higher temperatures, a faster rate of increase in temperature, as well as the capability to hold the fluid temperature constant for a short period of time without raising the device temperature significantly

in practical applications. It would be much easier to add feedback control of the microwave power if the temperature at a reference location was measured electronically rather than optically even if Rhodamine B or some other fluorescent dye was compatible with the other chemicals in the microchannel.

Finally, the growing concern that exposure to microwaves can be harmful to living cells may limit the ability to operate highly integrated lab-on-a-chip devices containing living microorganisms in conventional microwave ovens. On the other hand, the microwave field decreases rather rapidly away from a properly designed microscale microwave generator, potentially allowing live organisms and microwave transducers to co-exist on a lab-on-a-chip device. Our approach to establish temperature gradients appears to be especially well suited for thermal gradient focusing methods for analyte separations of cell metabolites in lab-on-a-chip devices. Other potential applications of integrated microwave heaters include cell lysis and PCR [50], as mentioned previously. The localized nature of on-chip microwave heating means that separate microwave heaters optimized for these different tasks could also co-exist on a single lab-on-a-chip device. Therefore, we believe that the technique outlined in this work will facilitate the application of microfluidics to other biological and chemical applications requiring spatial temperature gradients as well as to temperature gradient generation.

5. Conclusions

We have described a new robust technique to generate temperature gradients rapidly and selectively using an integrated microwave microfluidic device. The shape of the temperature profile can be adjusted by varying the microwave excitation frequency and the amplitude of the profile can

be adjusted by varying the microwave power. With our technique, the temperature gradients can be established locally and selectively by positioning the transmission line in the region of interest over the fluidic network.

The device used in this study offers several advantages. The heating elements are integrated with the microchannel so this device offers a portable platform for generating spatial temperature gradients. The device is simple, easy to use and allows for high frequency operation. The heating elements are easy to fabricate and the fabrication method is transferable to other microfluidic substrates. Reducing the thickness of the copper electrodes would provide larger temperature changes within the microchannel.

We predict that this approach can be scaled for high-throughput studies by fabricating multiple transmission lines in parallel, and that the absorption of Rhodamine B can be alleviated by modifying the surface to further improve the accuracy of fluid temperature measurements. Our approach to establish temperature gradients would be especially well suited for field gradient focusing methods for analyte separations. We also believe that the technique outlined in this paper will facilitate the application of microfluidics to a multitude of other biological and chemical applications requiring spatial temperature gradients.

Acknowledgments

This research was performed while JJS held a National Research Council (NRC) Research Associateship Award at the Electronics and Electrical Engineering Laboratory (EEL) of NIST. We thank J Atencia, S Leigh and B Nablo for helpful discussions. We also thank the Office of Science and Technology of the National Institute of Justice for providing part of the support for this work. Device fabrication was performed in part at the NIST Center for Nanoscale Science and Technology's Nanofab facility in Gaithersburg, MD.

References

- [1] deMello A J 2006 Control and detection of chemical reactions in microfluidic systems *Nature* **442** 394–402
- [2] Dittrich P S, Tachikawa K and Manz A 2006 Micro total analysis systems. Latest advancements and trends *Anal. Chem.* **78** 3887–907
- [3] Whitesides G M 2006 The origins and the future of microfluidics *Nature* **442** 368–73
- [4] Thorsen T, Maerkl S J and Quake S R 2002 Microfluidic large-scale integration *Science* **298** 580–4
- [5] Stone H A, Stroock A D and Ajdari A 2004 Engineering flows in small devices: microfluidics toward a lab-on-a-chip *Ann. Rev. Fluid Mech.* **36** 381–411
- [6] Duhr S and Braun D 2006 Why molecules move along a temperature gradient *Proc. Natl Acad. Sci. USA* **103** 19678–82
- [7] Arata H F *et al* 2005 Temperature alternation by an on-chip microheater to reveal enzymatic activity of beta-galactosidase at high temperatures *Anal. Chem.* **77** 4810–4
- [8] Mao H B, Yang T L and Cremer P S 2002 A microfluidic device with a linear temperature gradient for parallel and combinatorial measurements *J. Am. Chem. Soc.* **124** 4432–5

- [9] Tanaka Y et al 2000 Non-contact photothermal control of enzyme reactions on a microchip by using a compact diode laser *J. Chromatogr. A* **894** 45–51
- [10] Baaske P, Duhr S and Braun D 2007 Melting curve analysis in a snapshot *Appl. Phys. Lett.* **91** 133901
- [11] Mao H B et al 2002 Reusable platforms for high-throughput on-chip temperature gradient assays *Anal. Chem.* **74** 5071–5
- [12] Braun D and Libchaber A 2003 Lock-in by molecular multiplication *Appl. Phys. Lett.* **83** 5554–6
- [13] Dodge A et al 2004 A microfluidic platform using molecular beacon-based temperature calibration for thermal dehybridization of surface-bound DNA *Anal. Chem.* **76** 1778–87
- [14] Buch J S et al 2004 DNA mutation detection in a polymer microfluidic network using temperature gradient gel electrophoresis *Anal. Chem.* **76** 874–81
- [15] Huang T M and Pawliszyn J 2002 Microfabrication of a tapered channel for isoelectric focusing with thermally generated pH gradient *Electrophoresis* **23** 3504–10
- [16] Ross D and Locascio L E 2002 Microfluidic temperature gradient focusing *Anal. Chem.* **74** 2556–64
- [17] Zhang H D et al 2007 DNA mutation detection with chip-based temperature gradient capillary electrophoresis using a slantwise radiative heating system *Lab on a Chip* **7** 1162–70
- [18] Incropera F P and DeWitt D P 1990 *Fundamentals of Heat and Mass Transfer* 3rd edn (New York: Wiley)
- [19] Crews N, Wittwer C and Gale B 2008 Continuous-flow thermal gradient PCR *Biomed. Microdevices* **10** 187–95
- [20] Munson M S et al 2007 Temperature gradient focusing with field-amplified continuous sample injection for dual-stage analyte enrichment and separation *Anal. Chem.* **79** 6201–7
- [21] Matsui T et al 2007 Temperature gradient focusing in a PDMS/glass hybrid microfluidic chip *Electrophoresis* **28** 4606–11
- [22] Selva B, Marchalot J and Jullien M C 2009 An optimized resistor pattern for temperature gradient control in microfluidics *J. Micromech. Microeng.* **19** 065002
- [23] Shah J J et al 2007 Microwave dielectric heating of fluids in an integrated microfluidic device *J. Micromech. Microeng.* **17** 2224–30
- [24] Sundaresan S G et al 2005 Temperature control of microfluidic systems by microwave heating *Proc. Micro Total Analysis Systems 2005 (Boston, MA)*
- [25] Geist J et al 2007 Microwave power absorption in low-reflectance, complex, lossy transmission lines *J. Res. Natl Inst. Stand. Technol.* **112** 177–89
- [26] Kempitiya A et al 2009 Localized microwave heating in microwells for parallel DNA amplification applications *Appl. Phys. Lett.* **94** 064106
- [27] Marchiarullo D J et al 2007 Microwave-mediated microchip thermocycling: pathway to an inexpensive, handheld real-time PCR instrument *11th Int. Conf. on Miniaturized Systems for Chemistry and Life Sciences (2007, Paris, France)*
- [28] Sklavounos A et al 2006 Efficient miniaturized systems for microwave heating on microdevices *Proc. Micro Total Analysis Systems 2006 (Tokyo, Japan)*
- [29] Booth J C, M J, Janezic M, Baker-Jarvis J and Beall J A 2006 Broadband permittivity measurements of liquid and biological samples using microfluidic channels *IEEE MTT-S Int. Microwave Symp. (2006, San Francisco, CA)*
- [30] Facer G R, Notterman D A and Sohn L L 2001 Dielectric spectroscopy for bioanalysis: From 40 Hz to 26.5 GHz in a microfabricated wave guide *Appl. Phys. Lett.* **78** 996–8
- [31] Song C R, Harriss J E and Wang P S 2009 Compensating on-chip transmission line losses for a high-sensitivity microwave sensor *Sensors Actuators A* **154** 7–11
- [32] Song C R and Wang P S 2009 A radio frequency device for measurement of minute dielectric property changes in microfluidic channels *Appl. Phys. Lett.* **94** 023901
- [33] Ramos A et al 2009 Water flows induced by microwave electric fields in microsystems *J. Electrostat.* **67** 377–80
- [34] Ramos A et al 2009 Microwave-induced water flows in microsystems *Appl. Phys. Lett.* **94** 024104
- [35] Elibol O H, Reddy B and Bashir R 2008 Localized heating and thermal characterization of high electrical resistivity silicon-on-insulator sensors using nematic liquid crystals *Appl. Phys. Lett.* **93** 131908
- [36] Elibol O H et al 2009 Localized heating on silicon field effect transistors: device fabrication and temperature measurements in fluid *Lab Chip* **9** 2789–95
- [37] Issadore D et al 2009 Microwave dielectric heating of drops in microfluidic devices *Lab Chip* **9** 1701–6
- [38] Wiener V O 1890 Stehende Lichtwellen und die Schwingungsrichtung polarisirten Lichtes *Ann. Phys. Chem.* **40** 203–43
- [39] Bengtsson N E and Ohlsson T 1974 Microwave heating in the food industry *Proc. IEEE* **62** 44–55
- [40] Ramo S, Whinnery J R and Duzer V T 1993 *Fields and Waves in Communication Electronics* 3rd edn (Hoboken, NJ: Wiley)
- [41] Jargon J A, Marks R B and Rytting D K 1999 Robust SOLT and alternative calibrations for four-sampler vector network analyzers *IEEE Trans. Microw. Theory Tech.* **47** 2008–13
- [42] Ross D, Gaitan M and Locascio L E 2001 Temperature measurement in microfluidic systems using a temperature-dependent fluorescent dye *Anal. Chem.* **73** 4117–23
- [43] Samy R, Glawdel T and Ren C L 2008 Method for microfluidic whole-chip temperature measurement using thin-film poly(dimethylsiloxane)/Rhodamine B *Anal. Chem.* **80** 369–75
- [44] Siegel A C et al 2007 Microsolidics: fabrication of three-dimensional metallic microstructures in poly(dimethylsiloxane) *Adv. Mater.* **19** 727–33
- [45] Shah J J et al 2006 Capillarity induced solvent-actuated bonding of polymeric microfluidic devices *Anal. Chem.* **78** 3348–53
- [46] Hoebel S J et al 2006 Scanning temperature gradient focusing *Anal. Chem.* **78** 7186–90
- [47] Tolley H D et al 2002 Equilibrium gradient methods with nonlinear field intensity gradient: a theoretical approach *Anal. Chem.* **74** 4456–63
- [48] Pittman J L, Henry C S and Gilman S D 2003 Experimental studies of electro-osmotic flow dynamics in microfabricated devices during current monitoring experiments *Anal. Chem.* **75** 361–70
- [49] Shah J J et al 2006 Surface modification of poly(methylmethacrylate) for improved adsorption of wall coating polymers for microchip electrophoresis *Electrophoresis* **27** 3788–96
- [50] Shaw K J et al 2010 Rapid PCR amplification using a microfluidic device with integrated microwave heating and air impingement cooling *Lab Chip* **10** 1725–8